AD-766 244

FEASIBILITY STUDY OF EXOELECTRON IMAGING AS AN NDT METHOD FOR LASER SURFACE DAMAGE OF NONLINEAR OPTICAL MATERIALS AND LASER GLASS

Peter F. Braunlich, et al

Bendix Research Laboratories

Prepared for:

Air Force Cambridge Research Laboratories

March 1973

DISTRIBUTED BY:

NTIS

National Technical Information Service
U. S. DEPARTMENT OF COMMERCE
5285 Port Royal Road, Springfield Va. 22151

AFCRL – TR-73-0068

AD 766244

FEASIBILITY STUDY OF EXOELECTRON IMAGING AS AN NDT METHOD FOR LASER SURFACE DAMAGE OF NONLINEAR OPTICAL MATERIALS AND LASER GLASS

by
Peter F. Braunlich and John P. Carrico
Bendix Research Laboratories
Bendix Center
Southfield, Michigan 48076

Contract No. F19628-73-C-0032
Project No. 2042

Semi-Annual Technical Report No. 1

March 1973

Contract Monitor: John V. Nikula
Solid State Sciences Laboratory

Approved for public release; distribution unlimited.

Reproduced by
NATIONAL TECHNICAL
INFORMATION SERVICE
U S Department of Commerce
Springfield, VA 22151

Sponsored by
Defense Advanced Research Projects Agency
ARPA Order No. 2042

Monitored by

AIR FORCE CAMBRIDGE RESEARCH LABORATORIES
AIR FORCE SYSTEMS COMMAND
UNITED STATES AIR FORCE
BEDFORD, MASSACHUSETTS 01730

UNCLASSIFIED
Security Classification

DOCUMENT CONTROL DATA - R & D

(Security classification of title, body of abstract and indexing annotation must be entered when the overall report is classified)

1. ORIGINATING ACTIVITY (Corporate author) Bendix Research Laboratories Bendix Center Southfield, Michigan 48076	2a. REPORT SECURITY CLASSIFICATION Unclassified 2b. GROUP

3. REPORT TITLE

FEASIBILITY STUDY OF EXOELECTRON IMAGING AS AN NDT METHOD FOR LASER SURFACE DAMAGE OF NONLINEAR OPTICAL MATERIALS AND LASER GLASS

4. DESCRIPTIVE NOTES (Type of report and inclusive dates)

Scientific. Interim.

5. AUTHOR(S) (First name, middle initial, last name)

Peter F. Braunlich
John P. Carrico

6. REPORT DATE	7a. TOTAL NO. OF PAGES	7b. NO. OF REFS
March 1973	48	28

8a. CONTRACT OR GRANT NO F19628-73-C-0032 b. Project, Task, Work Unit Nos. 2042 n/a n/a c. DoD Element 62701E d. DoD Subelement n/a	9a. ORIGINATOR'S REPORT NUMBER(S) Semi-Annual Technical Report No. 1 6557, BRL Project 2422 9b. OTHER REPORT NO(S) (Any other numbers that may be assigned this report) AFCRL-TR-73-0068

10. DISTRIBUTION STATEMENT

A - Approved for public release; distribution unlimited.

11. SUPPLEMENTARY NOTES This research was sponsored by the Defense Advanced Research Projects Agency.	12. SPONSORING MILITARY ACTIVITY Air Force Cambridge Research Labs (LQ) L. G. Hanscom Field Bedford, Massachusetts 01730

13. ABSTRACT

This report presents the results of a 6-month effort on the development of an NDT method to predict surface damage on dielectric materials used in high power laser systems (such as those used in communication and ordnance). The research in this program has three objectives: investigating exoelectron (EE) properties of laser optical materials after exposure to ionizing or laser radiation; correlating exoelectron images with laser surface damage characteristics; and determining the feasibility of exoelectron surface imaging as an NDT method of predicting the laser surface damage threshold.

Results to date indicate that EE emission from laser glass is too weak and irreproducible to be of value. Experiments on pyroelectric $LiNbO_3$ led to the discovery of thermally stimulated field emission. This phenomenon is presently being attributed to a high electric field on the surface of a $LiNbO_3$ resulting from a small change in the temperature of the material.

DD FORM 1 NOV 65 1473

UNCLASSIFIED
Security Classification

KEY WORDS	LINK A		LINK B		LINK C	
	ROLE	WT	ROLE	WT	ROLE	WT
Pyroelectric materials						
Laser surface damage threshold						
$LiNbO_3$						
Laser glass						
Thermally stimulated field emission						
Exoelectron emission						
Laser optical materials						
Dielectric materials						

AFCRL – TR-73-0068

Copy No. ____

FEASIBILITY STUDY OF EXOELECTRON IMAGING AS AN NDT METHOD FOR LASER SURFACE DAMAGE OF NONLINEAR OPTICAL MATERIALS AND LASER GLASS

by
Peter F. Braunlich and John P. Carrico
Bendix Research Laboratories
Bendix Center
Southfield, Michigan 48076

Contract No. F19628-73-C-0032
Project No. 2042

Semi-Annual Technical Report No. 1

March 1973

Contract Monitor: John V. Nikula
Solid State Sciences Laboratory

Approved for public release; distribution unlimited.

Sponsored by
Defense Advanced Research Projects Agency
ARPA Order No. 2042

Monitored by

AIR FORCE CAMBRIDGE RESEARCH LABORATORIES
AIR FORCE SYSTEMS COMMAND
UNITED STATES AIR FORCE
BEDFORD, MASSACHUSETTS 01730

ic

ARPA Order No. 2042

Program Code No. 2D1

Contractor: Bendix Research Laboratories

Effective Date of Contract: 15 August 1972

Contract No. F19628-73-C-0032

Principal Investigator and Phone Number: Dr. Peter F. Braunlich
(313) 352-7725

AFCRL Project Scientist and Phone Number: John V. Nikula
(617) 861-3532

Contract Expiration Date: 14 February 1974

Qualified requestors may obtain additional copies from the Defense Documentation Center. All others should apply to the National Technical Information Service.

ABSTRACT

This report presents the results of a 6-month effort on the development of an NDT method to predict surface damage on dielectric materials used in high power laser systems (such as those used in communication and ordnance). The research in this program has three objectives: investigating exoelectron (EE) properties of laser optical materials after exposure to ionizing or laser radiation; correlating exoelectron images with laser surface damage characteristics; and determining the feasibility of exoelectron surface imaging as an NDT method of predicting the laser surface damage threshold.

Results to date indicate that EE emission from laser glass is too weak and irreproducible to be of value. Experiments on pyroelectric $LiNbO_3$ led to the discovery of thermally-stimulated field emission. This phenomenon is presently being attributed to a high electric field on the surface of a $LiNbO_3$ crystal resulting from a small change in the temperature of the material.

TABLE OF CONTENTS

	Page
SECTION 1 - INTRODUCTION	1
SECTION 2 - EXOELECTRON EMISSION FROM LASER MATERIALS - A LITERATURE REVIEW	3
2.1 Alkali Halides	3
2.2 Alkaline Earth Halides	4
2.3 Complex Compounds, Sulfides and Semiconductors	4
SECTION 3 - TEST FACILITY FOR MEASUREMENT OF GENERAL EXOELECTRON EMISSION PROPERTIES OF LASER MATERIALS	6
SECTION 4 - INVESTIGATIONS OF LASER GLASS	10
SECTION 5 - THE LASER SURFACE DAMAGE TEST FACILITY	15
5.1 Vacuum System	15
5.2 Laser System	15
5.3 Laser Beam Monitor System	16
5.4 The Electrostatic Emission Microscope	16
5.4.1 Optical System	19
5.4.2 Mechanical Layout [Figure 10(b)]	21
SECTION 6 - EXOELECTRON EMISSION FROM PYROELECTRIC MATERIALS	22
SECTION 7 - OUTLINE OF A THEORY OF EXOELECTRON EMISSION FROM NONPYROELECTRIC MATERIALS	31
SECTION 8 - FUTURE WORK	37
SECTION 9 - REFERENCES	38
SECTION 10 - TECHNICAL REPORT SUMMARY	41

Preceding page blank

LIST OF ILLUSTRATIONS

Figure No.	Title	Page
1	Schematic of Test System Comprising Electron Gun, Sample Holder, Channeltron®, and Photostimulation Capability	7
2	Photograph of Test System Comprising Electron Gun, Sample Holder, and Channeltron	8
3	Thermally-Simulated Exoelectron Emission from BeO	9
4	Exoelectron Imaging System	10
5	Thermally-Stimulated Exoelectron Emission from Laser Irradiated ED-2 Nd-Doped Glass Samples	12
6	Thermally-Stimulated Exoelectron Emission from ED-2 Nd-Doped Glass Sample	13
7	Thermally-Stimulated Exoelectron Emission from X-Ray Irradiated Nd-Doped Glass Samples	14
8	Experimental Arrangement of Laser Damage Test Facility	17
9	Vacuum Chamber and Sample Holder of Laser Damage Test Facility	18
10(a)	Potential Distribution in Electrostatic EE Microscope	20
10(b)	EE Microscope	20
11	Thermally-Stimulated Electron Emission from a Multidomain $LiNbO_3$ Crystal	23
12	Emission Image from Multidomain $LiNbO_3$ Single Crystals Photographed at Increasing Temperature (see Figure 11)	25
13	Emission Image from Multidomain $LiNbO_3$ Single Crystal (Same as in Figure 12); Photographed During Cooling	26
14	$LiNbO_3$ Single Crystal Used for Figures 12 and 13, Photographed After HF-Etch; Diameter of Crystal: 5/8 Inch	27
15	Schematic Dependence of the Spontaneous Polarization P_S on Temperature	28
16	Polarization of a Single Domain $LiNbO_3$ Crystal Upon Temperature Change	29

SECTION 1

INTRODUCTION

Previous work by the Bendix Research Laboratories established that thermally-stimulated exoelectron emission (TSEE) is observed from alkali halide crystals after the samples had been exposed to a single pulse of a high peak power Nd-glass laser.[1] Conventional TSEE glow curves, i.e., the dependence of the electron emission on the sample temperature, were measured. Also, with the aid of a unique new imaging technique, the distribution of the emission current density on the surface was recorded.[2]

Initial analysis of the observed phenomena indicated a relation between features of EE images and laser surface damage. Based on this, a research program was planned with the following overall objectives

- Investigation of exoelectron properties of a series of selected laser materials (glass, conventional nonlinear optical material, alkali halides) after exposure to ionizing radiation and high peak power laser radiation
- Systematic study of the relation between exoelectron images of the surface obtained after exposure to intense laser radiation and surface damage
- Investigation of the feasibility of establishing an NDT method for laser surface damage.

The specific program development areas include

(1) Screening experiments combined with a literature search to determine the types of optical laser materials that emit exoelectrons after exposure to ionizing radiation (e.g., X-rays, electrons of several keV kinetic energy)

(2) Extension of these experiments to laser-induced exoelectron emission.

(3) Establishing the required experimental facilities such as a well characterized ruby and/or Nd-glass laser, possibly a pulsed TEA-CO_2 laser, a test chamber, and improved exoelectron imaging devices, e.g., a suitable exoelectron microscope, in order to be able to use small laser diameters at high power density.

(4) Correlation of EE images with specific laser surface damage phenomena for common optical laser materials.

(5) Study of the abilities of the EE imaging technique to predict the surface damage threshold of such materials.

(6) Theoretical analysis of the physical processes involved in the formation of EE images after exposure of an optical material to a high peak power laser pulse.

The program described in this report is part of an extensive research effort presently in progress at the Bendix Research Laboratories. Related contracts are:

- "The Mechanism of Exoelectron Emission from Solid Surfaces," Air Force Office of Scientific Research, Arlington, Virginia, Contract No. F44620-72-C-0064.

  This project is mainly concerned with the exploitation of the Bendix exoelectron microscope as a tool in surface science. The goal is to better understand the mechanism of exoelectron emission from insulators and metals.

- "Exoelectron Studies of Surface Damage of Laser Materials," National Science Foundation, Contract No. GH-32606, to the Wayne State University, and subcontracted with the Bendix Research Laboratories.

  This particular project is concerned mainly with the underlying physical phenomena of the interaction of high peak power laser pulses with the surface of insulators and their correlation with the formation of the exoelectron image observed after exposure of the sample to the laser pulse.

  It is relevant to the work described in this report inasmuch as it will directly contribute to the understanding of the processes involved in the NDT method to predict surface damage thresholds of laser optical materials.

Related in-house programs are designed to support the above-mentioned efforts and to explore the possibilities of employing the exoelectron imaging technique for detection of structural damage associated with metal fatigue.

SECTION 2

EXOELECTRON EMISSION FROM LASER MATERIALS - A LITERATURE REVIEW

After successful demonstration of EE from pure LiF single crystals that had been exposed to high intensity laser pulses[1] it became important to investigate the EE properties of a series of materials that are of interest in connection with their use as components in high power lasers. We have therefore planned a program that consists of a detailed experimental schedule.

Even though EE properties of insulating solids have been, and continue to be, the subject of intensive investigations,[3] little is known about materials of laser interest and, except for the work by Bendix on LiF,[1] nothing was reported on EE from those materials after laser exposure.

The materials of interest include: alkali halides (mostly for IR windows and other optical components;, laser glass; certain sulfides, tellurides and selenides; alkaline earth halides; IR transparent mixed crystals (alkali halide mixtures); and nonlinear optical materials such as $LiNbO_3$, $Ba_2NaNb_5O_{15}$, KDP, $LiIO_3$, α-HIO_3, Ag_3AsS_3 and $LiHCO:H_2O$. This list is continuously growing as new laser optical materials are being developed. No work is reported in the literature on EE from any of the nonlinear materials or laser glass. Fairly extensive work has been reported on EE after excitation with ionizing radiation on alkali halides, some sulfides, and earth alkaline halides.

2.1 ALKALI HALIDES

Virtually all known alkali halides exhibit thermally-stimulated exoelectron emission (TSEE) or optically stimulated exoelectron emission (OSEE) after exposure to X-ray, short wavelength uv, fast electrons, and α-, β-, and γ-particles.[3] The glow peaks were observed in the range from liquid hydrogen temperature up to 600°C; most of the alkali halides emit quite intensely at temperatures above room temperature.[3] They are therefore all candidates for EE after exposure to intense laser light. However, in view of the fact that such materials as ED-2 glass and certain nonlinear crystals (e.g., $LiNbO_3$) are of greater interest at the present time, we have postponed the study of laser-induced EE emission from alkali halides to a later period of this contract. Experiments performed thus far on alkali halides were for the purpose of checking the performance of our EE test facility.

Of all alkali halides, LiF is the most intensely studied exoelectron emitter. Bohun[4] and Kramer[5] reported the same single glow peak at about 120°C that we observed after laser exposure.[1] Occasionally peaks at

higher temperatures were observed by various authors. These peaks are apparently due to different impurities present in the bulk as well as in the surface layer. The main peak at about 120°C has been diagnosed as being due to surface centers.[3] Extensive work has been done on Mn- and Ti-activated LiF powder, a material of particular interest to applications of EE to radiation dosimetry. However, owing to the scope of this project, we are not interested in intentionally doped materials but only those which are nominally pure. Therefore, we will not make use of reported EE work dealing with the effects of dopants. Of the remaining alkali halides, NaCl, KCl, and KBr have been studied.[6] Glow peaks at 500 to 545°K of all three materials have been found to be due to traps that were identified as F-centers. Other peaks at temperatures below room temperature have been found; they are, however, of no interest here because any NDT method for laser surface damage should be based on EE peaks above 25°C. In the course of our test program, we have found that pure NaCl (obtained from Harshaw, Cleveland, Ohio) is a good EE emitter after bombardment with 3 keV electrons.

2.2 ALKALINE EARTH HALIDES

Three members of this group, namely, CaF_2, SrF_2, and BaF_2 are of interest as laser optical materials and have been studied with respect to their exoelectron emission properties. Nominally, pure CaF_2 emits usually around 200 to 240°C.[7,8] The thermal activation energy of the 240°C peak was determined to be 1.03 eV.[8]

BaF_2 exhibits EE peaks at 125°C, 180°C, and 320°C, and the glow peaks of SrF_2 were found to be at 118°C, 253°C, and 383°C.[9]

2.3 COMPLEX COMPOUNDS, SULFIDES AND SEMICONDUCTORS

The materials comprise a large group of compounds whose exoelectron properties have been studied in some detail.[3] Some of these are of laser interest such as calcite, ZnS, ZnSe, CdTe, special glasses, and some semiconductors, as well as a group of compounds used in reflection or antireflection coatings. However, aside from some results on semiconductors,[10] all work reported is of rather limited value for our purpose. The reason for this lies in the fact that the exoelectron emission properties depend to a large extent on the method of preparation and on the impurity content. Since production methods for alkali halides, earth alkaline halides, and semiconductors are now standardized, fairly reproducible qualities of pure crystals can be readily obtained. This is not the case, however, for most of the compounds considered in this subsection. We therefore refrain at this point from a reivew of EE data reported in the literature. Most compounds are expected to be exoelectron emitters. Laser glass, ferroelectric materials, and, most notably, pyroelectric materials play a special role among the complex compounds and are of particular interest with respect to their extensive use in high power laser applications. We therefore selected $LiNbO_3$ (representative of the pyroelectric-ferroelectric group) and ED-2 laser glass as the first materials for

our initial experimental studies. The results of the work on glass and initial work on lithium niobate are reported in subsequent sections of this report.

SECTION 3

TEST FACILITY FOR MEASUREMENT OF GENERAL EXOELECTRON EMISSION PROPERTIES OF LASER MATERIALS

A schematic of the test apparatus is given in Figure I. Figure 2 shows a photograph of this system which was developed to facilitate the collection of data on laser material. As indicated in Figure 1, the system consists of a sample holder, an electron gun, a photostimulation system, and a channel electron multiplier. This system is mounted in a Balzer's oil diffusion pump high vacuum station. Typical operating pressures are in the low 10^{-7} Torr range.

Samples are easily fastened to the holder with good thermal contact. Both heating and cooling capability are provided. A thermocouple is used to monitor sample temperature. The electron gun is a pentode configuration with two-dimensional deflection capability. Its spot size, intensity, and energy are adjustable. This gun permits us to outgas samples and fill traps under vacuum. Thus, we are able to study general exoelectron phenomena on the samples without opening the system to air for X-ray treatment. This procedure is both cost- and time-saving. Of course, when necessary, samples irradiated by X-rays or the laser can also be studied. The photostimulation system consists of a high intensity Bausch and Lomb monochromator, a window into the vacuum, and appropriate optical collimation and focusing. This capability permits us to investigate nonlinear optical materials without interference from high energy electrons produced by thermally induced field emission (see Section 6).

The channel electron multiplier and detection electronics provide wide dynamic range capability for obtaining data on samples ranging from very weak emitters such as glass to strong emitters such as BeO. In the scheme shown in Figure 1, the electron multiplier is used in a pulse counting mode. Each detected exoelectron gives rise to a high gain pulse which is integrated and displayed.

Figure 3 shows exoelectron emission intensity as a function of temperature for BeO. The traps were filled by bombardment with 3 keV electrons. The integrator output and sample temperatures as measured by a theromcouple are displayed on a two-channel strip chart recorder. Similar data have been collected for ED-2 Nd-doped glass and NaCl crystals. In the situation where the emission intensity is very weak, the electron multiplier output pulses can be counted and stored in a 400-channel analyzer. The log amplifier and divider shown in Figure 1 enable us to record directly the log of the emission intensity as a function of 1/T on an x-y recorder so that activation energies can be readily determined.

Preceding page blank

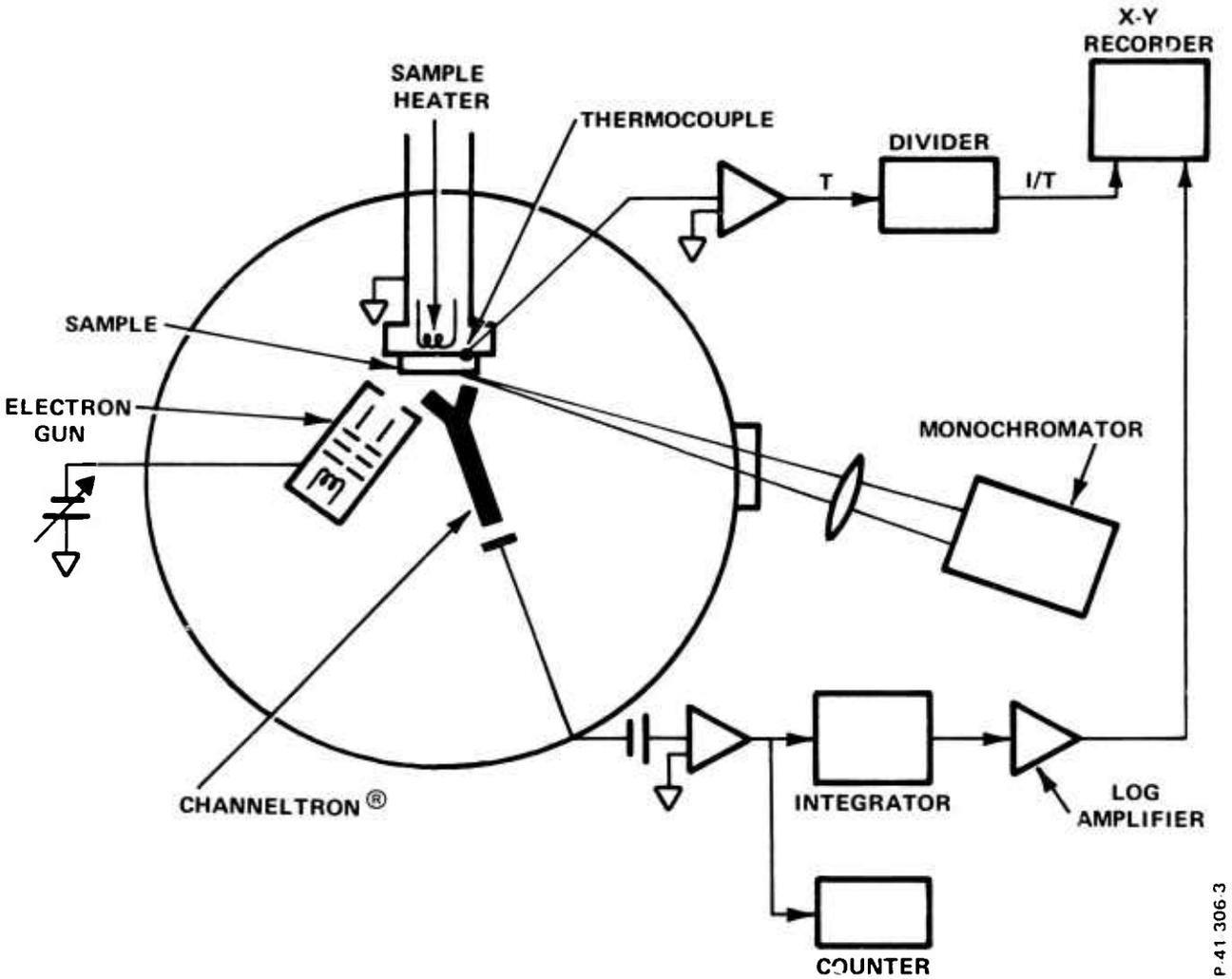

Figure 1 - Schematic of Test System Comprising Electron Gun, Sample Holder, Channeltron®, and Photostimulation Capability

Figure 2 - Photograph of Test System Comprising Electron Gun, Sample Holder, and Channeltron

The test facility also includes exoelectron imaging capability. This consists of a microchannel electron multiplier array and phosphor screen. The phosphor display can be recorded on film or monitored using a photomultiplier. The latter arrangement was used to obtain the data on ED-2 Nd-doped glass reported in Section 5. The photomultiplier also permits us to obtain thermoluminescence data.

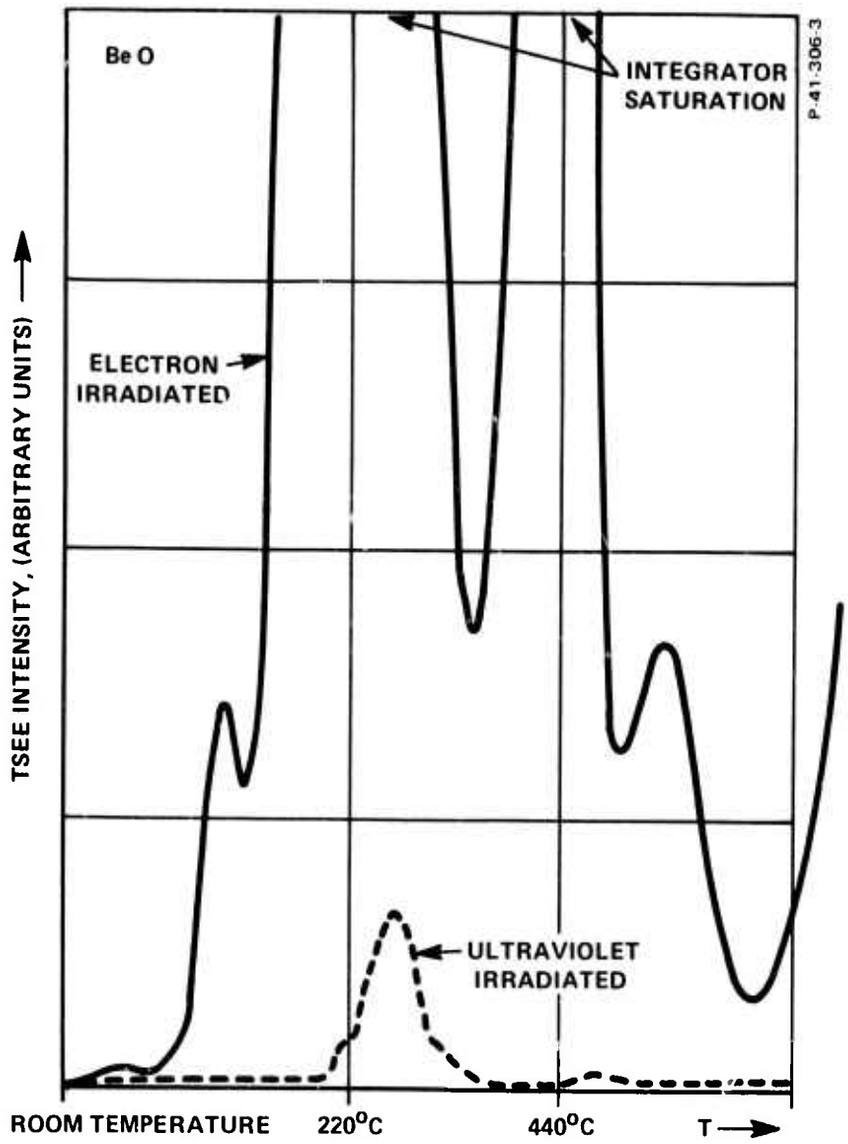

Figure 3 - Thermally-Simulated Exoelectron Emission from BeO

SECTION 4

INVESTIGATIONS OF LASER GLASS

It was deemed important to study Nd-doped glass because of its use in laser systems. Also, nothing is known about exoelectron emission from glassy compounds except for some work by Becker[11] and Gourge.[12,13] Becker[11] observed that radiation-induced thermally-stimulated exoelectron emission was much stronger from crystalline than from glassy lithium borate. Thermally-stimulated emission from quartz glass and from silver activated phosphate glass was measured by Gourge.[12,13]

Because of Becker's work,[11] it was expected that there would be little or no emission from glass. Accordingly, the detection system was designed to measure weak emission. The system shown in Figure 4 was used

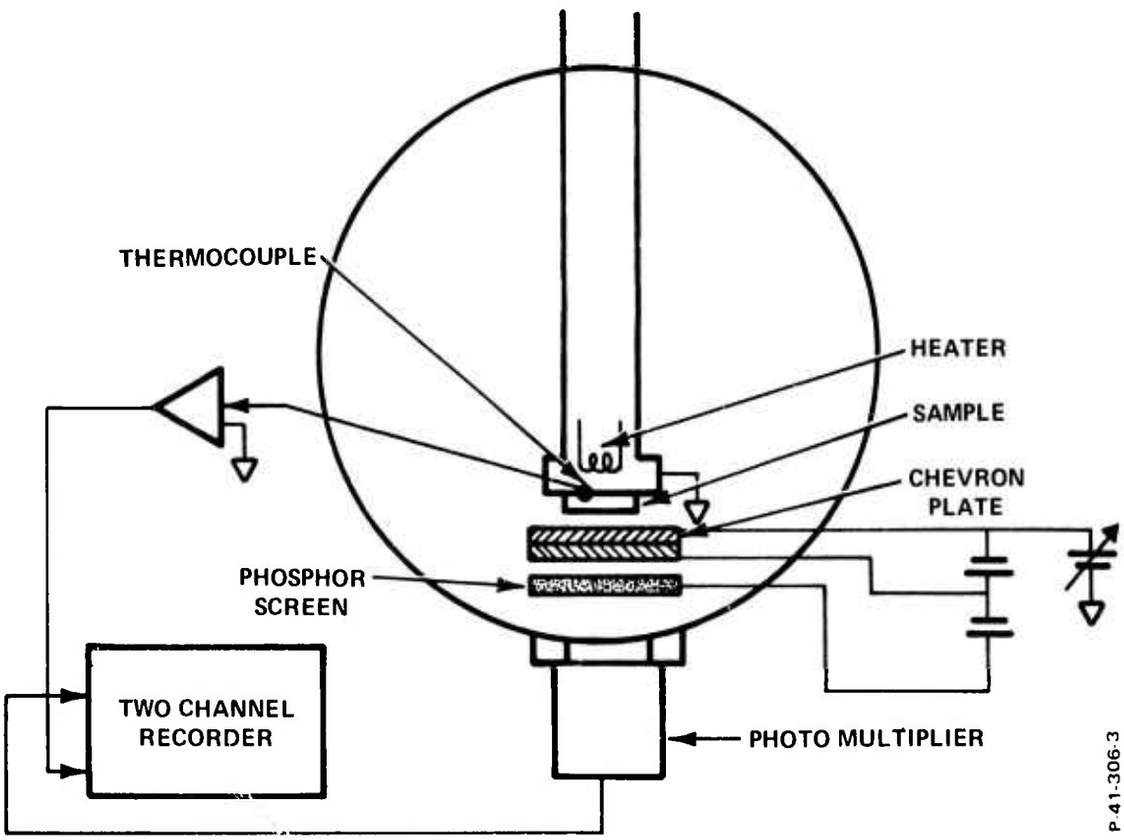

Figure 4 - Exoelectron Imaging System

in early work. It consisted of a microchannel electron multiplier and phosphor screen which could be read out visually or by means of a photomultiplier. More recently, the channel electron multiplier scheme shown in Figure 1 was used.

ED-2 Nd-doped glass samples (1/2" x 1/2" x 1 mm) were ordered from Owens-Illinois. These samples were of optical quality and prepared (polished and cleaned) by Owens-Illinois. Six of these samples were then exposed to the Owens-Illinois high intensity Nd-glass laser operated in the TEM_{00} mode. Each sample was exposed to a different laser intensity. The intensities ranged from slightly above the threshold for damage [110 J/cm^2 for 25 ns (FWHM) pulse] to about 10 percent of damage threshold. These irradiated samples were then packaged in dry ice in order to minimize depopulation of traps (if any) and brought to the Research Laboratories for measurement. Care was exercised in the handling of the samples to prevent possible bleaching by ambient light. Figure 5 shows the results of exoelectron measurement for these samples; the percents indicated on these curves denote the percent of the threshold intensity for damage. The system shown in Figure 4 was used to obtain these data. The detector was operated at very high gain. The exoelectron emission from these samples above room temperature was very weak. Furthermore, as evident for the glow-curves of Figure 5, the emission cannot be correlated with previous exposure of the sample to high peak powers of laser light.

Other tests were then conducted to further investigate the exoelectron properties of ED-2 Nd-doped glass. A sample from the original Owens-Illinois batch was measured for emission. This sample was of the same quality and was prepared in the same way as those discussed above, except that it was not exposed to laser light. The exoelectron intensity is shown in Figure 6 as a function of temperature during the first heating of this sample. Also shown is the background which was obtained during a second heating. This sample was then irradiated with X-rays (65 kV - 15 mA) and again measured (third heating - Figure 6). In another test, four samples from the original batch and not irradiated with laser light were exposed to X-rays and then measured. The glow curves are shown in Figure 7. These results again point up the difficulties encountered with glass.

Further tests on this original batch from Owens-Illinois included laser irradiation with the Bendix Korad (K-1) focused ruby laser operated Q-switched in a multi-transverse mode. Laser intensities ranging from below to well above damage were used. No exoelectron emission was observed either visually (imaging) or with photomultiplier readout.

A second batch of samples was obtained and exposed to laser light by Owens-Illinois. The results were as irreproducible and uncorrelated as before. Finally, a sample from this second batch was inserted into the system shown schematically in Figure 1. The exoelectron emission was measured as a function of temperature after electron bombardment. It was not possible to obtain reproducible results.

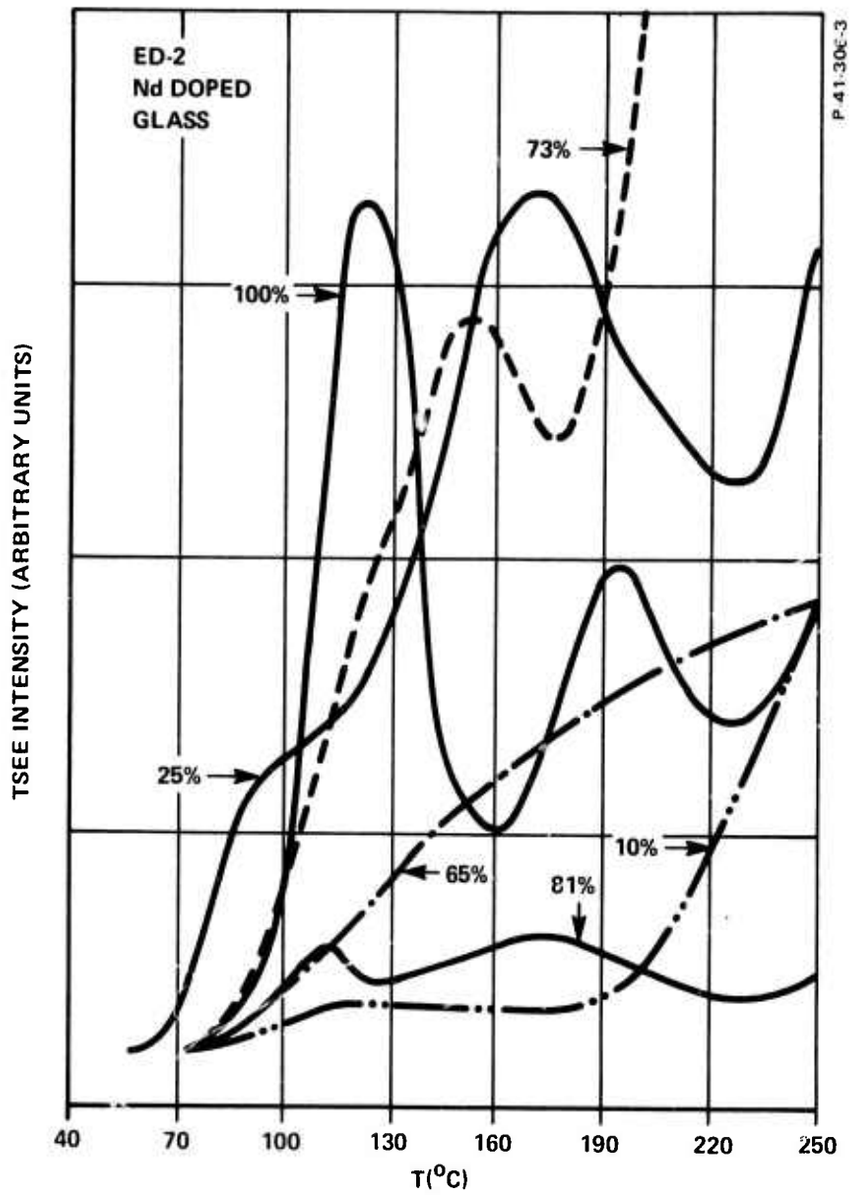

Figure 5 - Thermally Stimulated Exoelectron Emission from Laser Irradiated ED-2 Nd-doped glass samples

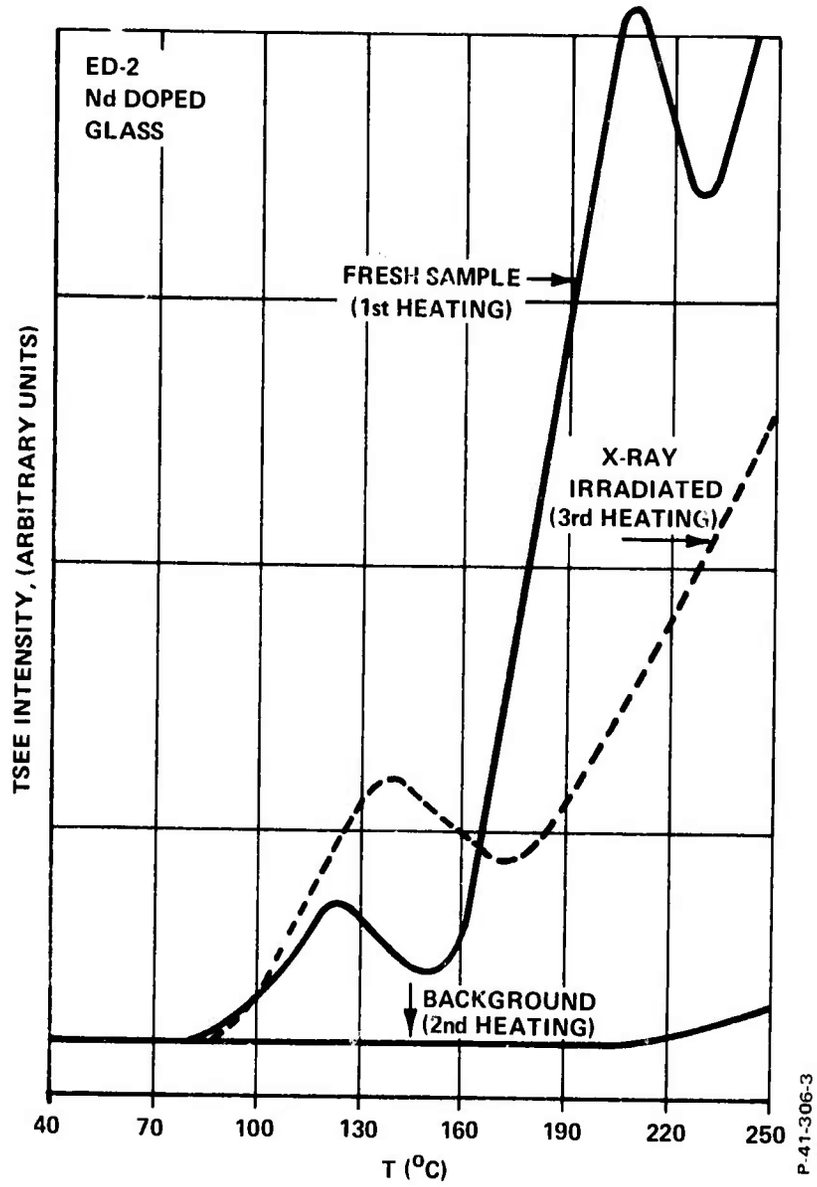

Figure 6 - Thermally-Stimulated Exoelectron Emission from ED-2 Nd-Doped Glass Sample

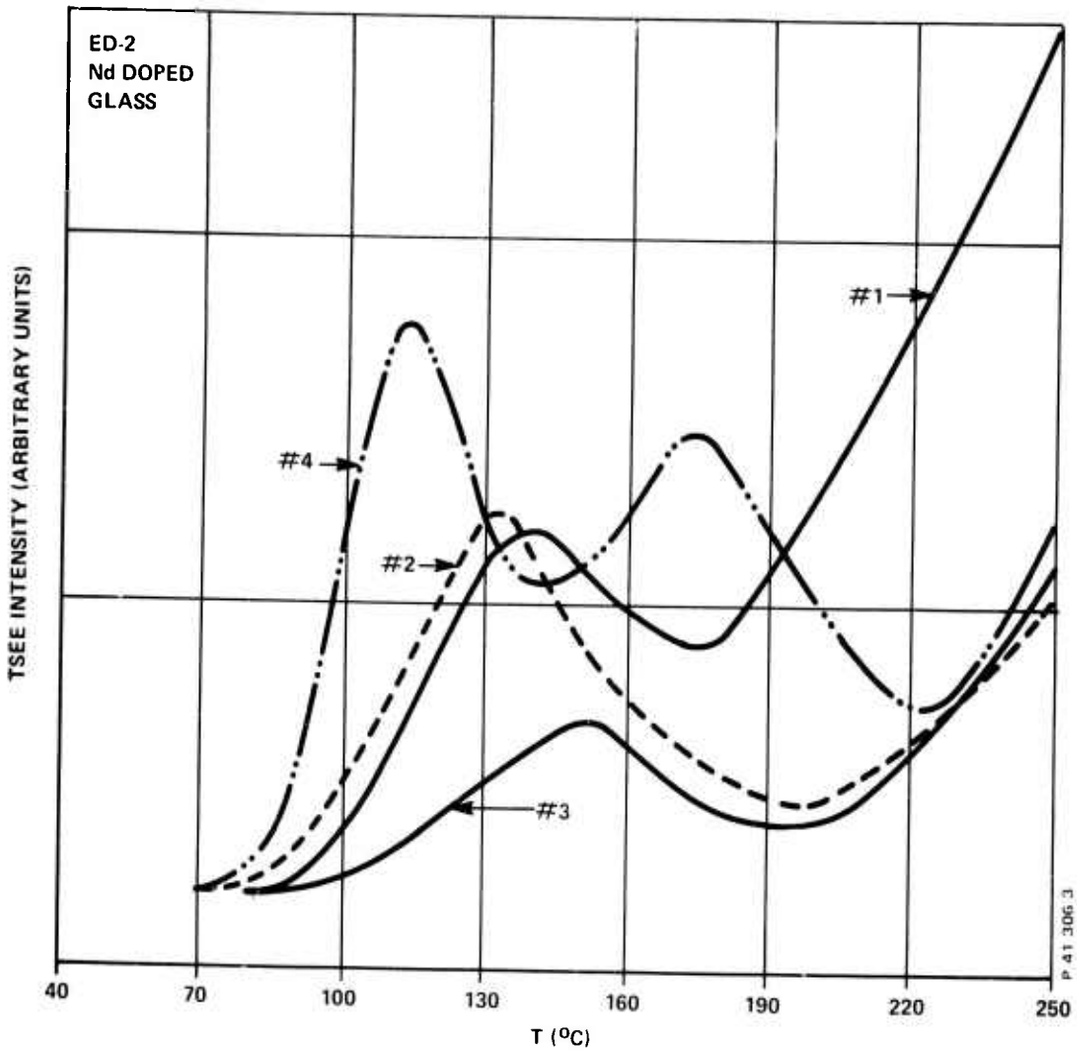

Figure 7 - Thermally-Stimulated Exoelectron Emission from X-Ray Irradiated Nd-Doped Glass Samples

SECTION 5

THE LASER SURFACE DAMAGE TEST FACILITY

The experimental techniques which are employed in the study of the precursors of laser surface damage were described in References 1 and 14. The so-called exoelectron imaging technique permits the investigation of the spatial distribution of electrons that are emitted from the irradiated surface upon heating or by optical stimulation. These electrons are released from electron traps in a thin surface layer. The exoelectron emitting surface is imaged directly with the aid of a multichannel electron multiplier of high spatial resolution, or an electron immersion lens (exoelectron microscope) can be used in order to obtain magnified images.[14] Direct imaging is employed whenever the laser power density is sufficiently high over a spot size of several millimeters in diameter. Since the ruby and Nd-glass lasers available in our laboratory permit spot sizes up to about 100 μm in the TEM_{00} transverse mode, the exoelectron microscope is required in most of our studies.

In the reporting period we have concentrated on the design and construction of an electron microscope that is suitable for the intended studies. This microscope is an improved version of the simple instrument described in Reference 14. Furthermore, we have redesigned our laser system in order to obtain Q-switched pulses of TEM_{00} mode. A major portion of our effort was devoted to the construction of a clean high vacuum chamber and a sample holder that is appropriate for the complex sample manipulation which will be required. In addition, an alignment system based on a He-Ne laser was established. In the following sections we describe the experimental setup in more detail.

5.1 VACUUM SYSTEM

After an unsuccessful attempt to use existing vacuum equipment, we obtained a Balzer's pump system which was disassembled, cleaned, reassembled, and then isolated to eliminate mechanical vibration. We also constructed an experimental chamber. In order to keep this chamber oil-free, a double cryopump system was connected for rough pumping. A liquid N_2 trapped diffusion pump produces a working pressure 5×10^{-7} Torr or better.

5.2 LASER SYSTEM

Since the optical table laser system and the pump experimental chamber system are independent, an alignment system had to be developed in order to provide a precise location of the high power laser beam with respect to the sample. The chamber is fixed on a three-stage table which permits linear movement in two directions normal to the incident beam and

Preceding page blank

rotation around a vertical axis normal to the beam. Close tolerances of 0.001 inch or less in the dimensions guarantee accurate movement and adjustment (Figures 8 and 9).

There are several lasers available for our project:

- He-Ne Laser: This laser serves as an alignment tool which simulates the beam of the high power laser.
- Korad Laser (type K-1): This laser, Q-switched with the aid of a bleachable dye, may be operated with a Nd-glass rod or a ruby rod emitting in excess of 100 MW power (multimode). For the experiments we tuned the plane-mirror cavity in order to achieve a TEM_{00} mode operation of about 5 MW power output.

5.3 LASER BEAM MONITOR SYSTEM

(1) Temporal Distribution of the Beam: A fast photodiode (ITT 4000) with a rise time of 0.65 ns and a fast oscilloscope (Tektronix 519) are used to measure the time distribution of our Q-switched pulses.

(2) Spatial Distribution: The spatial distribution is measured in a photometric manner. The beam is divided by a beam splitter. The split beams are focused by identical lenses. One beam is focused onto the sample and the other onto a microscope lens operating as a projector lens. The microscope lens produces an enlarged image of the focal spot on a photographic plate. Curves of equal intensity will be traced by a microdensitometer.

5.4 THE ELECTROSTATIC EMISSION MICROSCOPE

We will now describe briefly the simple electrostatic microscope, which is similar in design to the one described by K. Kanaya et al.[15] At present, our instrument is used as a one-stage system consisting only of the objective lens. However, the mechanical parts are constructed so that a projector lens can be added with little effort if the requirement arises. The magnification of the instrument using the objective lens alone is on the order of 100 X, which is sufficient for most of the work planned for this instrument. Those factors which determine the image quality, particularly the focal properties, spherical and chromatic aberrations, are analytically derived from theoretical models of the three-electrode lens introduced by Glaser and Schiske,[16] Lippert and Pohlit[17] and Kanaya et al.[18]

For the design of the specimen manipulator, we took into consideration the fact that the vacuum chamber and the sample holder must permit imaging as well as proximity imaging. This feature required a specimen manipulator which is independent of the microscope. Up to four samples can be heated simultaneously up to 300°C with our manipulator. The

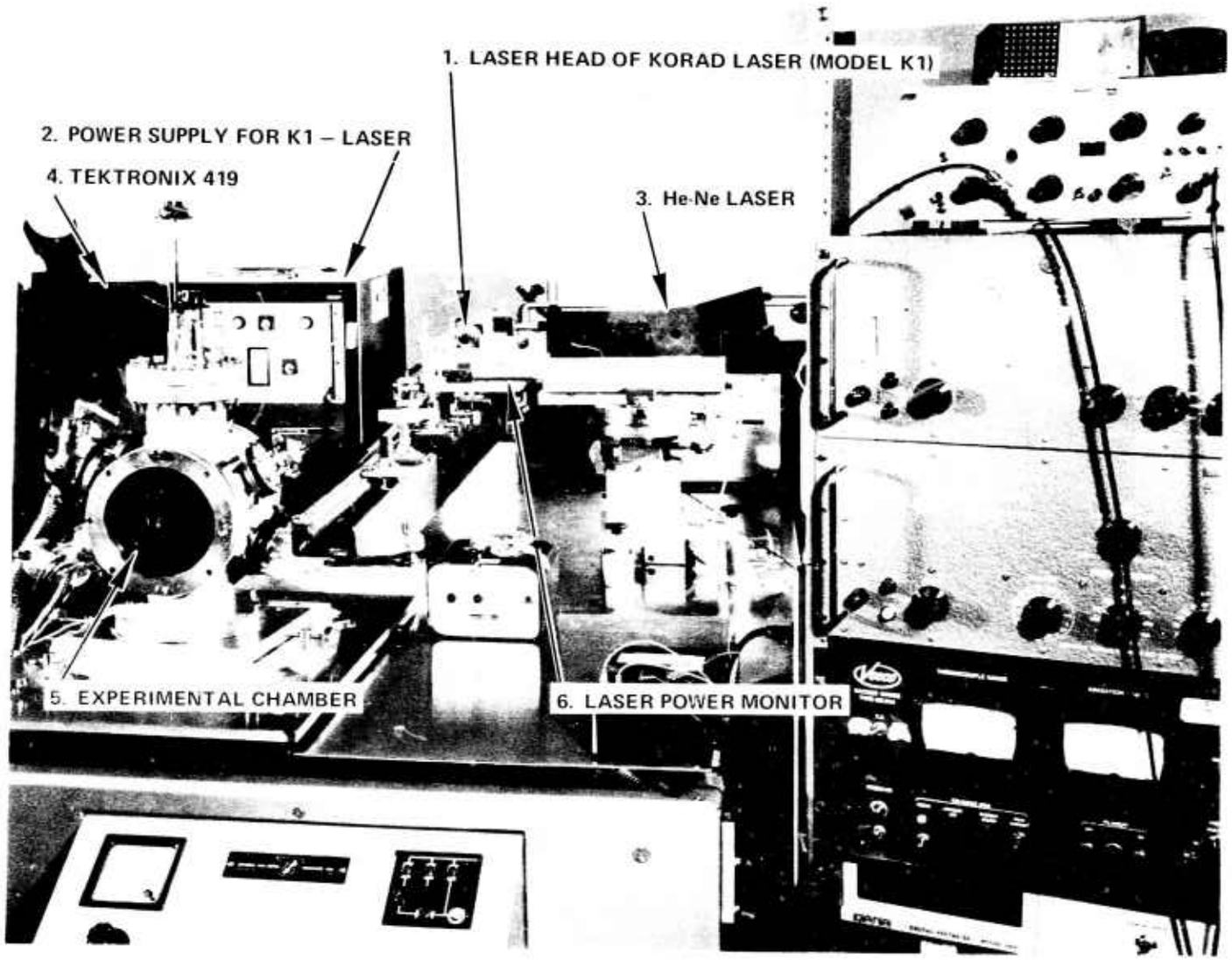

P 41 306 3

Figure 8 – Experimental Arrangement of Laser Damage Test Facility

P 41-306-3

Figure 9 - Vacuum Chamber and Sample Holder of Laser Damage Test Facility

sample holder can be cooled with air, liquid N_2, or water. The samples can be moved simultaneously in two directions perpendicular to the optical axis.

5.4.1 Optical System

Considering the bell-shaped potential distribution of the three-electrode lens developed by Glaser and Schiske,[16] one can derive all optical parameters simply as functions of two characteristic parameters, the half-width d of the bell-shaped potential and the ratio k^2 of the center potential of the lens to the accelerating potential [Figure 10(a)]. Both are functions of the lens dimensions. In order to simplify the construction, a lens type was chosen where all electrodes have apertures of equal diameter. The central electrode is considered to be thin compared to the distance between the outer electrodes. To match the parameters d and k^2 with these initial conditions, one starts out with a formula by Regenstreif[19]

$$\phi(z) = V_1 + \frac{V_2 - V_1}{B}\left[B' - (z + z_2)\arctan\left(\frac{z + z_2}{R_2}\right)\right.$$

$$\left. - (z - z_2)\arctan\left(\frac{z - z_2}{R_2}\right) + 2z\arctan\left(\frac{z}{R_1}\right)\right] \qquad (3)$$

where

$$B = B' - 2z_2\arctan\left(\frac{2z_2}{R_2}\right) + 2z_1\arctan\left(\frac{z_2}{R_1}\right) + R_2 \qquad (4)$$

$$B' = (z + z_2)\arctan\left(\frac{z_1 + z_2}{R_2}\right)$$

$$+ (z_1 - z_2)\arctan\left(\frac{z_1 - z_2}{R_2}\right) + 2R_1 \qquad (5)$$

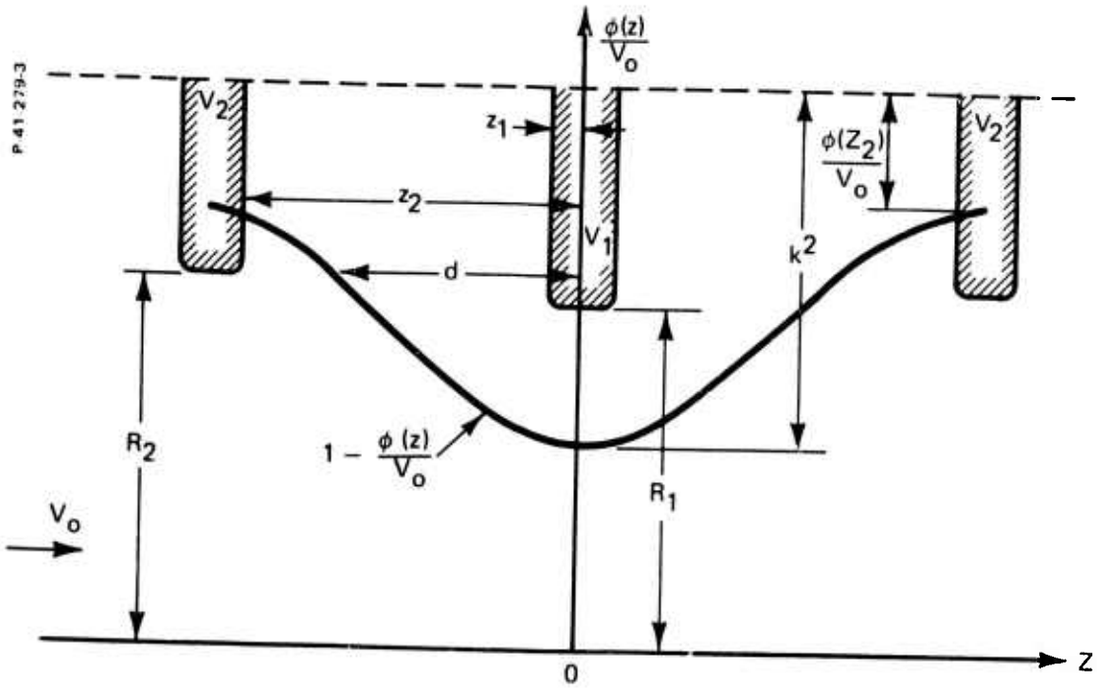

Figure 10(a) - Potential Distribution in Electrostatic EE Microscope

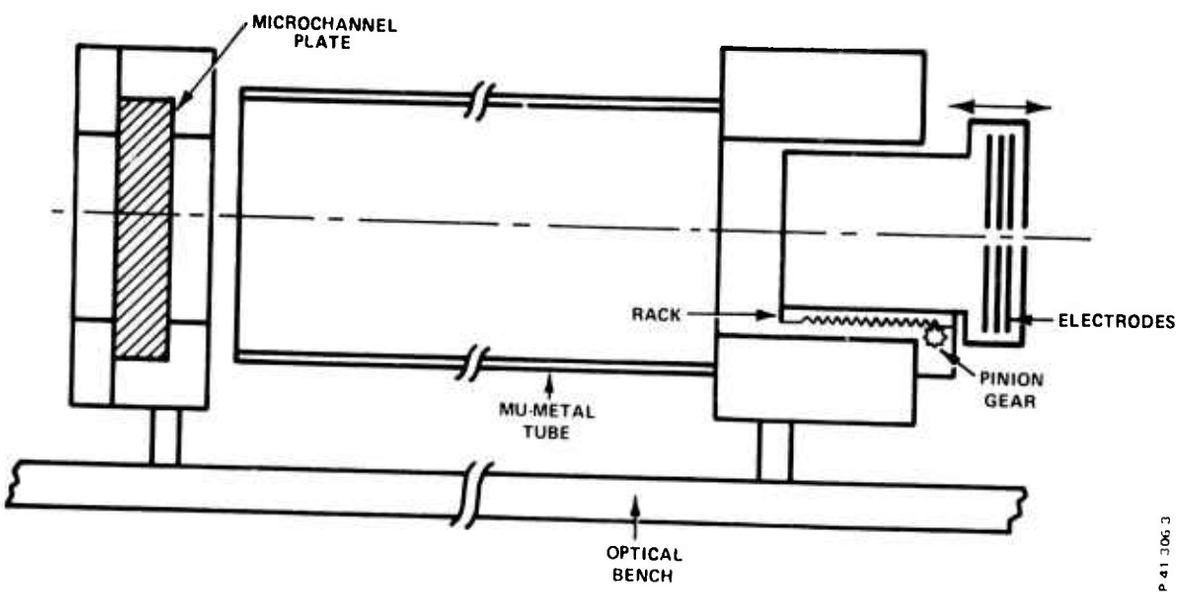

Figure 10(b) - EE Microscope

For an aperture diameter ($R_1 = R_2$) of R = 0.050 inch and an electrode distance of z_2 = 0.1 inch, one obtains values for

$$k^2 = \frac{\phi(o)}{V_o} = 0.75 \quad \text{and} \quad d = 0.068 \text{ inch}$$

$$z_1 = 0.012 \text{ inch}$$

The voltage ratio V_2/V_1 is assumed to be 2.25.

In this case, the focal length f turns out to be f = 0.2 inch using the calculation method suggested by Kanaya et al.[15]

5.4.2 Mechanical Layout [Figure 10(b)]

The design of the instrument was governed mainly by two considerations: the microscope should be (a) usable in a UHV-system without modifications, and (b) easy to disassemble and reassemble.

In order to minimize outgassing, all parts were made of stainless steel; pump-out holes were provided wherever possible and necessary. The lens structure was made of soft iron for magnetic shielding purposes. For the same reason, a "Mu-Metal" shielding is used for the field-free shift region between the lens and the detector. Since the sample holder is fixed in the direction parallel to the optical axis, it is necessary that the lens move to permit optimal focusing. The translational movement is accomplished by a rack and pinion gear combination which is connected to a rotatable vacuum feedthrough. The lens structure moves in a high-precision oil-free ball bearing which permits one to take out the lens chamber and reassemble the microscope again without serious realignment.

SECTION 6

EXOELECTRON EMISSION FROM PYROELECTRIC MATERIALS

Pyroelectric crystals change their spontaneous polarization P_s when their temperature changes. The resulting electric fields are known to influence exoelectron emission.[20] Optically-stimulated exoelectron emission from TGS (triglycine sulfate) and Rochelle salt was found to be affected by the ferroelectric polarization of these materials.[20] In air, field-induced electron emission from Seignette salt and ceramic barium titanate was observed[21] and explained by localized high electric fields on the surface which resulted in the ionization of the nitrogen in the air. These experiments indicate that ferroelectric and most notably pyroelectric materials constitute a special class of materials with respect to their exoelectron emission properties. Any work that aims at understanding of the mechanism of exoelectron emission from insulators must pay special attention to these materials.

All experiments reported so far on ferroelectric and pyroelectric crystals were done in air and they are therefore not reproducible.[21] For this reason, we have performed a series of experiments in vacuum (10^{-6} Torr). We selected $LiNbO_3$ single crystals which were poled in an electric field and therefore consisted of a single domain or revealed, after etching in HF, a well defined domain structure. All surfaces examined were perpendicular to the c-axis, the axis of polarization. The crystals were nominally pure. As a result of this investigation, we now understand exoelectron emission from pyroelectric materials. By slowly heating the crystals from room temperature to about 100°C, we measured electron emission current densities of 10^{-10} to 10^{-9} A/cm^2 (averaged over the sample surface). Depending on the direction of the c-axis (either c^+ or c^-), a similar effect was observed upon cooling. Multidomain samples (nearly circular domain boundaries in the crystal surface perpendicular to the c-axis) emitted upon cooling, as well as upon heating. This type of exoelectron emission, observed for the first time, may be called thermally-stimulated field emission of electrons (TSFE). A typical emission curve is shown in Figure 11. The temperature of the sample was varied according to the curve shown at the top of this figure; the corresponding electron emission current is shown on the botton.

TSFE turned out to be a useful means for imaging the surface of the crystal. We have obtained simple proximity images with the aid of a closely packed bundle of electron multipliers, each 50 μm in diameter. The emitted electrons are multiplied in this device and projected onto a phosphor screen. The spatial variations in emission current density

Preceding page blank

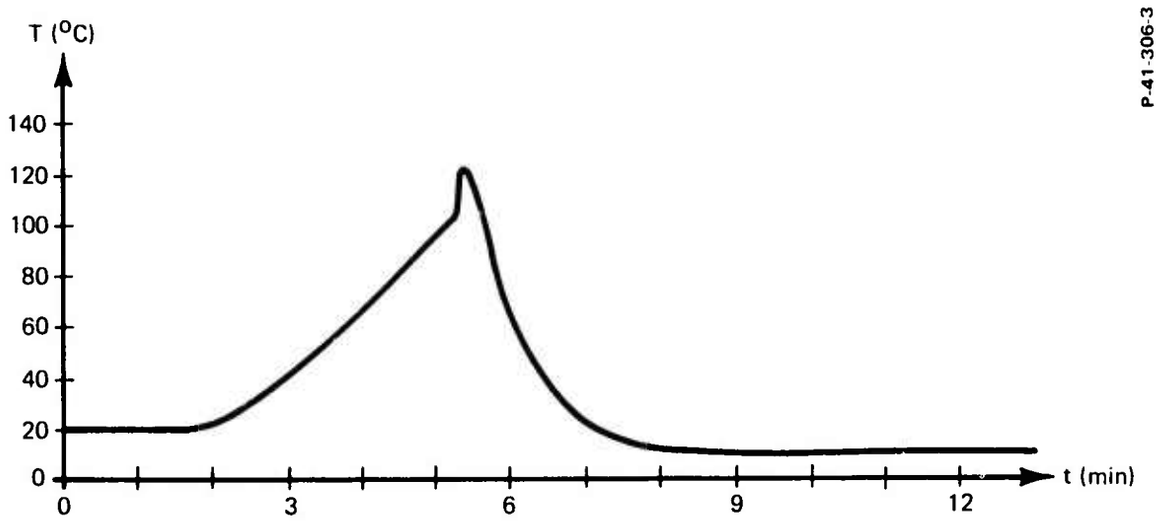

(a) Temperature Curve

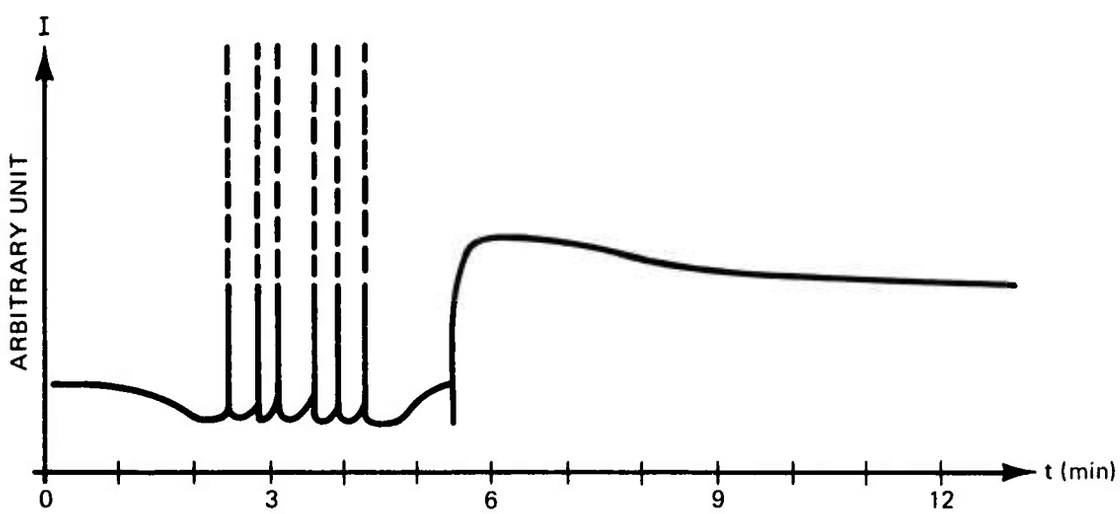

(b) Corresponding Emission Current

Figure 11 - Thermally-Stimulated Electron Emission from a Multidomain $LiNbO_3$ Crystal

could be easily displayed in this manner with a resolution of about 300 μm. The image obtained when the front of the multiplier bundle was only 2 mm above the crystal surface showed quite clearly the structure of the ferroelectric domain. Typical TSFE images of a multidomain $LiNbO_3$ crystal are shown in Figures 12 and 13. Figure 14 is a photograph of the same crystal after etching in HF.

Because of the strong emission of charged particles upon heating or cooling of a pyroelectric crystal such as $LiNbO_3$, conventional thermally-stimulated exoelectron emission after exposure of the sample to ionizing radiation could not be observed. Therefore, in order to study traps in such materials, optically-stimulated exoelectron emission has to be used.

As indicated above, the mechanism of TSFE from $LiNbO_3$ is field emission of electrons. The theory of this effect has to explain the existence of electric fields that are strong enough ($\geq 10^7$ V/cm) to cause such emission.

Pyroelectric crystals have a spontaneous polarization P_S below the Curie temperature T_c. In the case of $LiNbO_3$, $P_S = 0.7$ C/m^2 at room temperature and $T_c \approx 1200°C$ (see Figure 15). Due to this polarization, the c-faces of the crystal are charged with a surface charge of density η_i, and we have the relation $P_S = \eta_i$. The resulting field is $|E_i| = 4\pi\ \eta_i = 4\pi\ |P_S|$ [Figure 16(a)].

When the crystal is placed between the grounded heating block [Figure 16(b)] and the microchannel plate, a field E_0 develops such that we might consider the surface charge η_i to be induced by that field. The relation between η_i and $|E_0|$ is

$$\eta_i = \frac{\varepsilon - 1}{4\pi\ \varepsilon}\ |E_0|\ . \tag{6}$$

To derive this relation, we assume that the surface charges η_i originate from the difference between E_0 in front of the crystal and a field E_ε inside it such that $E_0 - E_\varepsilon = 4\pi\ \eta_i$. The dielectric displacement vectors inside and in front of the crystals are equal, and therefore we have the additional relation $\varepsilon E_\varepsilon = E_0$. Equation (6) is readily obtained from this and we finally have

$$E_0 = 4\pi\ \frac{\varepsilon}{\varepsilon - 1}\ P_S \approx 4\pi\ P_S\ . \tag{7}$$

($\varepsilon = 50$ for $LiNbO_3$ along the c-axis).

Figure 12 - Emission Image from Multidomain $LiNbO_3$ Single Crystals Photographed at Increasing Temperature (see Figure 11)

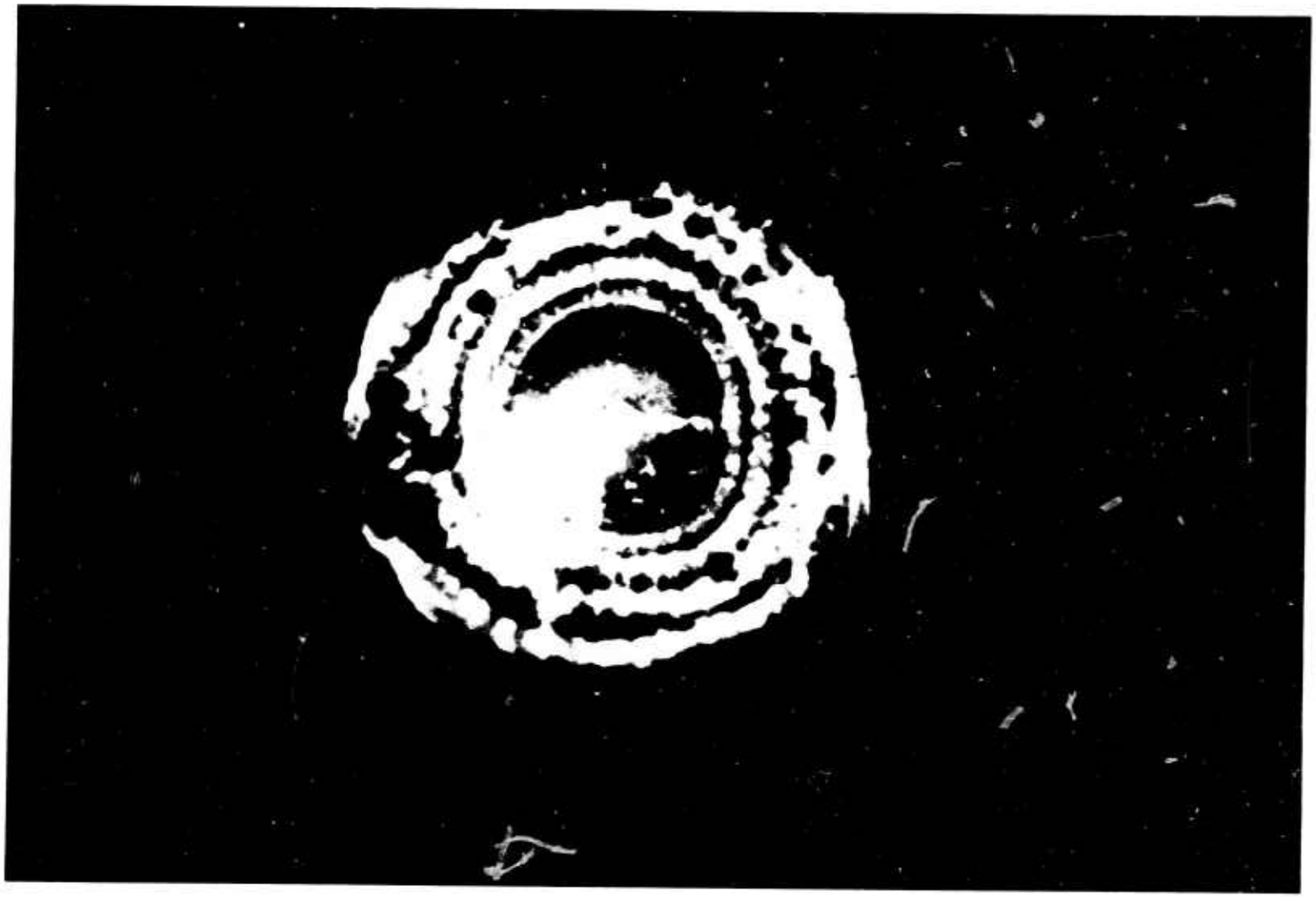

Figure 13 - Emission Image From Multidomain $LiNbO_3$ Single Crystal (Same as in Figure 12); Photographed During Cooling

Figure 14 - $LiNbO_3$ Single Crystal Used for Figures 12 and 13, Photographed after HF-Etch; Diameter of Crystal: 5/8 Inch

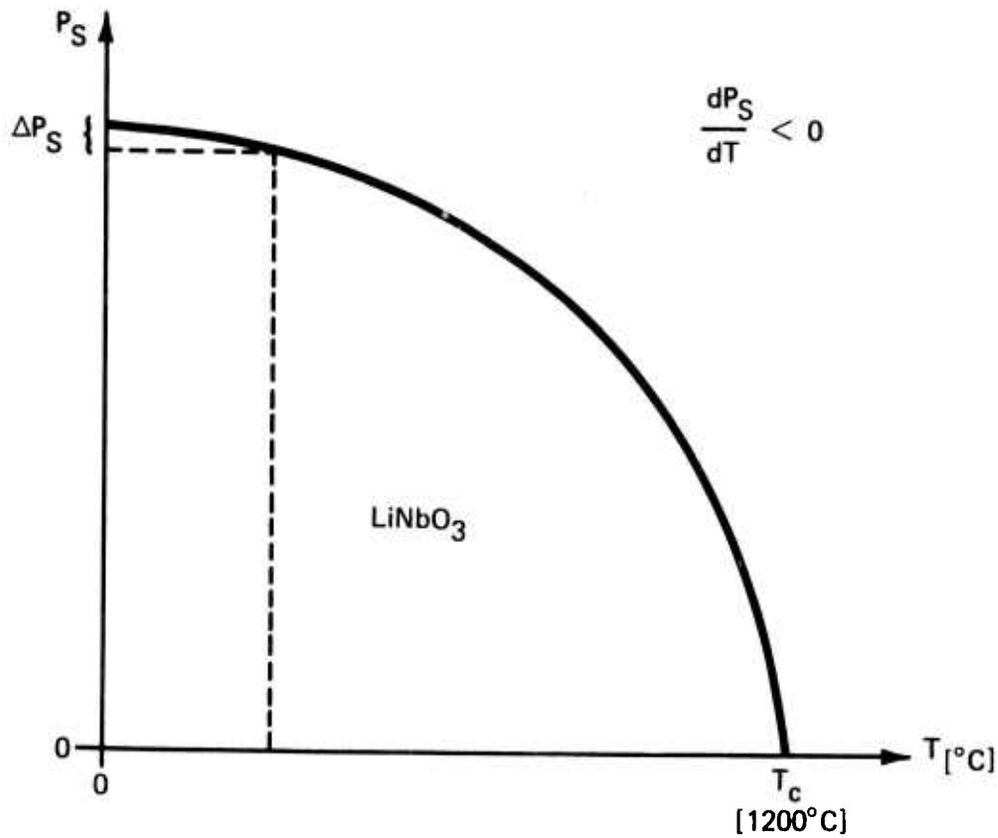

Figure 15 - Schematic Dependence of the Spontaneous Polarization P_S on Temperature

The field E_i causes compensation of the surface charges η_i in any real crystal because of its finite conductivity σ. In air, additional compensation occurs by ions that move from the surrounding atmosphere onto the crystal surface. In vacuum, the decay of η_i is given by $\eta_i = \eta_i\ (\tau = o)\ \exp\ (-\varepsilon t/\sigma)$. As a result, the surface charge of a pyroelectric crystal is compensated completely after $t >> \sigma/\varepsilon$.

Experimentally, one can observe pyroelectric properties only by changing the crystal temperature at a rate that is characterized by a time constant smaller than σ/ε. In our experiments, σ/ε was typically 30 minutes or more. We started with a compensated crystal and, by changing its temperature, generated a change in spontaneous polarization ΔP_S (Figure 15). This results in a field $E_0 \approx 4\pi\ \Delta P_S$. Assuming that we changed P_S by only 1 percent, that is, $\Delta P_S = 0.01$, $P_S = 7 \times 10^{-3}\ C/m^2$, we obtain, using the relation $1\ C \hat{=} 9 \times 10^{11}$ V cm, a field perpendicular to the surface of the crystal $E_0 = 7.9 \times 10^6$ V/cm, which is

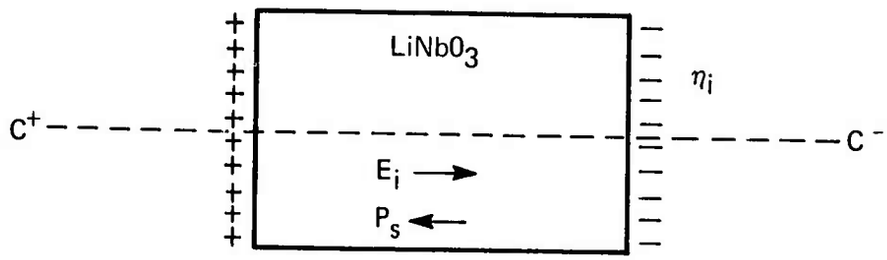

(a) In vacuum

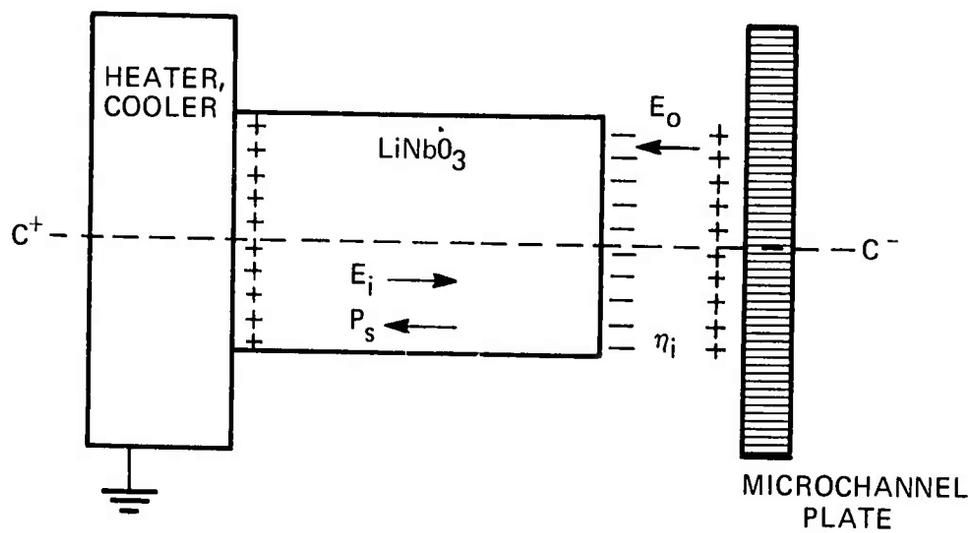

(b) Between the heating block and the microchannel plate in vacuum

Figure 16 - Polarization of a Single Domain $LiNbO_3$ Crystal Upon Temperature Change

sufficient to cause field emission of electrons. Fields of this strength will also exist between different domains (regions of opposite orientation of the c-axis at the surface). The microchannel plate intercepts part of the emitted electrons, and the typical images of Figures 12 and 13 are formed.

The observations made on $LiNbO_3$ appear to be of some significance in explaining certain aspects of laser surface damage of pyroelectric crystals as well as in the experimental methods to be employed in our further investigations.

The observation of TSEE after laser exposure of pyroelectric materials is not possible because TSFE will, in general, be a much stronger effect not only when c-faces are investigated, but the strong fields generated will make the observation of TSEE from other crystal faces difficult if not impossible. For the release of trapped carriers, photons have to be used (OSEE). A uniform light beam of low power density will be employed in the work on pyroelectric materials planned for the remaining contract period.

The implications of TSFE and the associated electric field, which is sufficiently strong to modify the surface by emission of charged particles, are of particular interest. We will focus on this aspect of laser surface damage in future investigations. We expect the generation of strong electric fields to be due not only to free carriers (photoexcitation),[22] but also to a rise in temperature upon exposure of the crystal to high peak power laser pulses. This is especially true for "imperfect" surfaces. Small increases in temperature will cause sufficient changes in polarization to generate strong electric fields. In initial experiments, we have observed electron emission from the spot of the crystal that was exposed to one pulse from a ruby laser having a power density sufficient for surface damage. The c-face of a single domain $LiNbO_3$ crystal was viewed through the imaging device (microchannel plate plus phosphor screen) a few seconds after exposure. The emission was clearly visible for about 30 s. Problems encountered with the imaging device delayed these experiments somewhat. However, we were able to overcome these difficulties, and our experimental program is proceeding again according to the planned schedule.

SECTION 7

OUTLINE OF A THEORY OF EXOELECTRON EMISSION FROM NONPYROELECTRIC MATERIALS

Exoelectron emission measurements constitute an excellent means for probing traps at or near the surfaces of solids. The basis for probing traps is the expectation that the one or more links exist between laser-generated free carriers and the traps. The carriers, produced by multiphoton processes, are free to absorb laser energy and accelerate to energies capable of avalanche ionization. Evidence for this free carrier generation comes from photoemission and photoconductivity measurements. The link between the traps and the laser-generated free carriers is that the traps act to "freeze out" a portion of the free carriers.[23] This portion is then measured by thermal or optical stimulation of the traps. Exoelectron images obtained in LiF at laser power densities above and somewhat below the surface damage threshold feature a characteristic ring shape.[1]

In addition to a "freezing out" of free carriers, the traps may act as intermediate levels for multiphoton generation of the carriers and, in the case of resonance, increase the cross sections for the processes. Another possibility for trap involvement is that populated traps may act as electron donors for ensuing avalanche processes.

The theory of exoelectron emission from an insulating solid exposed to intense laser radiation has to describe the features of the exoelectron images obtained in such experiments. Each experiment consists of two distinctly different phases:

(1) The exposure of the sample to the laser pulse: The solid interacts with the photon field. Electrons are redistributed over available electron levels by such processes as multiphoton ionization, recombination, trapping, photoemission, avalanche ionization, and thermal transitions. In this phase, a small number of electrons are trapped in metastable levels. Only those traps that are in a thin surface layer have to be considered for exoelectron studies. The spatial distribution of the trapped electrons is a map of the spatial distribution of the conduction electrons which were generated during the laser pulse.

(2) The subsequent heating of the exposed sample (thermally-stimulated exoelectron emission): The probability for thermal release of the trapped electrons increases with increasing temperature. A small portion of the electrons released from the traps overcomes the work function barrier and is emitted as exoelectrons into the vacuum.

Preceding page blank

The theory to be developed has to provide the link between the processes occurring during the time of the laser exposure and the intensity distribution of the exoelectron emission image.

At high laser power densities, the physical processes involved are identical to the processes occurring during laser surface damage. The investigation of exoelectron emission after exposure of the sample to intense laser light below the surface damage threshold is of importance because it deals with processes that apparently are precursors of laser surface damage and therefore are likely to shed light on laser breakdown of transparent material.

The seemingly impossible task to analyze these various processes has been simplified considerably by recently published quantitative work on multiphoton excitation of conduction electrons[24] and on the nature of laser breakdown in alkali halides,[25] one of the more important classes of materials to be considered in this research project.

Multiphoton absorption must be considered the most important source of conduction electrons during the duration of the laser pulse,[24] and avalanche ionization has now been identified as the prevailing mechanism of laser breakdown in alkali halides[25] at laser power densities above the damage threshold. Aside from this, it is now established that the theory of dc dielectric breakdown[26] of these materials is applicable without major modification to ac electric fields of optical frequency.

In the following we will use an electron kinetics approach to describe the spatio-temporal behavior of the density of conduction electrons in both experimental phases described above. The parameters, entering the set of electron rate equations that will be developed, will be discussed. Our goal is to either measure these parameters in the course of the experimental work or to obtain them from the literature and to compare the experimental results with theoretical values. Rate equations of the type to be discussed here can be found in an article by Franz.[27]

The energy levels of an insulating solid are, in the simplest case, described by a band model. In thermal equilibrium and in the absence of radiation, the electrons occupy the completely filled valence band. All trap levels and the conduction band can be assumed empty. Denoting the concentration of conduction electrons as n_c, the concentration of trapped electrons in N traps as n_t, and the concentration of electrons in the valence band as n_v, and neglecting for the time being diffusion of electrons and any dc electric fields, we can write

$$\frac{dn_c}{dt} = n_c\,\omega_i + n_v\,\omega_{vc} + n_t\,\omega_{tc} - n_c\,(n_c + n_t)\,\omega_{cv} - n_c\,(N - n_t)\,\omega_{ct} \qquad (8)$$

$$\frac{d_{nt}}{dt} = n_v\,(N - n_t)\,\omega_{vc} + n_c\,(N - n_t)\,\omega_{ct} - n_t\,(n_c + n_t)\,\omega_{tv} - n_t\,\omega_{tc} \qquad (9)$$

where the ω_{ik}'s are the transition probabilities in appropriate units. The subscripts designate the transitions (e.g., ω_{cv} is the transition probability for an electron in the conduction band to reach the valence band, etc.); ω_i is the avalanche ionization probability.

Charge neutrality is required and therefore the number of holes in the valence band is equal to $n_c + n_t$. A correction for emitted electrons from a thin surface layer is neglected at this point. It is important to point out that all electron concentrations and transition probabilities are functions of the coordinates z (along the axis of the laser beam and perpendicular to the entry surface of the sample) and r (the radial distance from the beam axis),as well as the time t.

The avalanche ionization rate ω_i pertains only to the ionization of valence electrons and does not include ionization of filled traps. Franz does not consider this process.[26,27] We will come back later to this important question.

Only traps that are in a surface layer of thickness δ (escape depth of the exoelectrons) participate in the formation of the exoelectron image in the phase 2 experiment. The goal of the theory is therefore to calculate n_t $(t_p, r, 0 \leq z \leq \delta)$, where t_p is the time duration of the laser pulse. In order to do this, we must know the transition probabilities ω_{ik}, all of which depend on the spatio-temporal characteristics of the laser beam, that is the dependence of the laser photon flux on t, r, and z. Furthermore, the temperature T of the sample enters as an important parameter and it also will be a function of these variables.

Transitions of electrons between the bands and the impurity levels (traps) are due to different processes. The avalanche ionization rate ω_i has been the subject of several theoretical calculations[27] and, in a recent paper by Yablonovitch and Bloembergen,[25] it was shown that the theory of dc-avalanche ionization is applicable also to laser photon fields by staightforwardly converting the photon flux density to the equivalent rms field strength E. The authors report the field dependence of ω_i in the case of NaCl for laser frequencies from the infrared to the frequency of the ruby laser. Their calculations can be extended to other alkali halides as well. All other remaining transitions are of either thermal origin or are caused by recombination and single or multiphoton absorption.

Field emission of electrons from the valence band or the traps, an important process in dc-dielectric breakdown, is of course absent in electric fields of optical frequencies.

The transition probabilities ω_{ik} in Equations (8) and (9) contain contributions from optical transitions and thermal transitions. Using the superscripts o and th to distinguish between these two processes, we have

$$\omega_{tc} = \omega_{tc}^{th} + \omega_{tc}^{o} \tag{10}$$

$$\omega_{vc} = \omega_{vc}^{th} + \omega_{vc}^{o} \tag{11}$$

$$\omega_{vt} = \omega_{vt}^{th} + \omega_{vt}^{o} \tag{12}$$

Since, in our case, the traps are expected to be at most 2 eV below the lower edge of the conduction band, the energy difference between the upper edge of the valence band and the traps is large in wide band gap materials such as alkali halides. We may therefore safely neglect ω_{vt}^{th} and ω_{vc}^{th} at laser photon fluxes below the onset of catastrophic avalanche ionization. The thermal transition probabilities may be expressed in terms of the spontaneous recombination probabilities. Of importance is the relation

$$\omega_{tc}^{th} = 2\ \omega_{ct} \left(\frac{m^* k T}{2\pi \hbar} \right)^{3/2} \exp\ (-E/k T) \tag{13}$$

where E is the trap depth and m^* the effective electron mass at the bottom of the conduction band. The transition rate ω_{cv} is known from the lifetime of free carriers.

In wide band gap insulators, ω_{vc}^{o} is a multi-photon transition and requires special consideration. The most recent description of multi-photon absorption in various alkali halides was given by Catalano et al.[24] They give a summary of theoretical and experimental results which we will use in the course of this research project. The transition probability per unit time for N-photon absorption is given by

$$\omega_{vc}^{o} = \sigma_N\ f\ (z)^N \tag{14}$$

where σ_N is the cross section for N-photon absorption, measured in cm^{2N} sec^{N-1}, and f(z) a function which describes the z-dependence of the laser photon flux.

Assuming that single photon absorption from impurity levels is a process that is much weaker than multiphoton absorption, the z-dependence of the laser flux is calculated from the equation

$$d\ f\ (z) = -\ \alpha_N\ f\ (z)^N\ d\ z \tag{15}$$

The absorption coefficient α_N is given by

$$\alpha_N = \sigma_N / n_v \tag{16}$$

The concentration of valence electrons n_v is equal to the density of active atoms in the solid. The solution of Equation (15) is

$$f(z) = F_o \left[1 + (N - 1) F_o^{N-1} \right] \alpha_N z^{1/(1-N)} \qquad N > 1 \tag{17}$$

Equation (7) is correct only for a laser flux that is not sufficient to initiate avalanche ionization. The absorption coefficient changes as soon as avalanche ionization is initiated. The absorption coefficient α_i due to free carrier absorption was given by Yablonovitch and Bloembergen:[25]

$$\alpha_i = 4 \pi e^2 \tau_i n_c \left[c\, n_r\, m^* \left(1 + \omega^2 \tau_i^2 \right) \right]^{-1} \tag{18}$$

where

e = electron charge

τ_i = collision time

ω = frequency of the laser light

n_r = linear refractive index of the sample

c = velocity of light

Even though the role of free carrier absorption (α_i) is generally acknowledged to be a dominant one in laser induced breakdown of transparent dielectrics, it is at the moment still uncertain whether an avalanche ionization is required or not. Hellworth[28] argues that enough energy can be absorbed before electrons gain the kinetic energy required for ionization. Assuming the ionization avalanche is launched, the free carrier concentration n_c grows exponentially with time and we have

$$n_c = n_c(o) \exp \left[\int_o^t \omega_i \, dt \right] \tag{20}$$

as one can see from Equation (8).

Due to the absorption of laser photons, the temperature of the sample will change and influence all the thermal transition probabilities, especially ω_{tc}^{th}, which determines the concentration of electrons remaining in the traps after the laser pulse has hit the sample. To come back to the importance of trap ionization by electrons, this process appears to be present. However, up to this point, we have not been able to find relevant information on this effect. The knowledge of it is of course necessary in order for us to evaluate the characteristic exoelectron images that are obtained after the sample was subjected to a high power laser pulse.

In the forthcoming report period, we will attempt to include such effects as carrier diffusion, temperature effects, and trap ionization by electron collision in order to complete the set of rate equations (8) and (9) and to solve them for n_t $(t_p, r, 0 \leq z \leq \delta)$.

The exoelectron experiment (phase 2) involves simply heating the sample with a linear heating rate and the detection of exoelectrons $n_e(r)$ emitted from the sample with high spatial resolution (exoelectron image). The theory of thermally stimulated exoelectron emission will then be used to find the connection between $n_e(r)$ and n_t (t_p, r, z).

SECTION 8

FUTURE WORK

The research program for the next six-month contract period is as follows:

(1) Continuation of screening experiments on general exoelectron properties of selected laser optical materials.

(2) Measurement of optically stimulated exoelectron emission from $LiNbO_3$ and possibly one or two other nonlinear optical materials after exposure to ionizing radiation (electrons or X-rays) and/or high peak power laser radiation.

(3) Completion of tests on thermally-stimulated field emission from $LiNbO_3$ subsequent to exposure to high peak power laser pulses.

(4) Continuation of exoelectron imagery of surfaces of optical materials that had been subjected to high peak power laser pulses.

(5) Continued development and improvement of experimental techniques for nondestructive prediction of laser surface damage of optical materials.

SECTION 9

REFERENCES

1. P. Bräunlich, Appl. Phys. Lett., 20, 4 (1972).

2. P. Bräunlich, Appl. Phys., 42, 496 (1971).

3. K. Becker, "Exoelectron Emission from Insulating Solids" in Critical Reviews in Solid State Science, (Chemical Rubber Co., Cleveland, Ohio, 1972), Vol. 3.

4. A. Bohun, Czech. J. Phys., 12, 328 (1962).

5. J. Kramer, Acta Phys. Austriaca, 10, 327 (1957).

6. V. Bichivin and H. Kääbre, PTB-Mitt., 80, Vol. 5 (1970).

7. J. Dolejsi, J. Kanturek, A. Bohun, and J. Trnka, Czech. J. Phys., 8, 548 (1958).

8. B. Sujak and A. Gieroszyuski, Acta Phys. Polonica, 32, 541 (1967).

9. B. Sujak and S. Gasior, Acta Phys. Polonica, 33, 231 (1968).

10. A. Scharmann, "Electronennachemission in Festkorperprobleme VI," (Vieweg Verlag, Braunschweig, 1966), O. Madelung ed.

11. K. Becker, CONF-680920,200 (1968).

12. G. Gourgé and W. Hanle, Acta Phys. Aust., 10, 427 (1957).

13. G. Gourgé, Z. Phys., 153, 186 (1958).

14. P. Bräunlich, B. Rosenblum, J. P. Carrico, L. Himmel, and P. K. Rol, Appl. Phys. Lett., 22, 61 (1973).

15. K. Kanya, H. Kawakatsu, H. Yamazaki, and S. Sibata, J. Sci. Instr., 43, 416 (1966).

16. W. Glaser and P. Schiske, Optik, 11, 422 (1954).

17. W. Lippert and W. Pohlit, Optik, 10, 447 (1953); 11, 181 (1954).

18. K. Kanya et al., Optik, 21, 399 (1964).

Preceding page blank

19. E. Regenstreif, Ann. Radioelect., 6, 51 and 6, 114 (1951).

20. L. M. Belayev and G. G. Bendrikova, Fiz. Trerdogo Tela, 6, 645 (1964).

21. B. Sujak and J. Kusz, Acta Phys. Polonica, 28, 491 (1965).

22. W. D. Johnston, Jr., J. Appl. Phys., 41, 3279 (1970).

23. P. Kelly, Phys. Rev. B., 5, 749 (1972).

24. I. M. Catalano, A. Cingolani, and A. Minafra, Phys. Rev. B., 5, 1629 (1972).

25. Eli Yablonovitch and N. Bloembergen, Phys. Rev. Lett., 29, 907 (1972).

26. W. Franz, Zschrft. f. Physik, 132, 285 (1942).

27. W. Franz, Handbuch der Physik XVII, 153 (1956), S. Flugge ed., Springer, Berlin.

28. R. W. Hellwarth, Nat. Bur. Stand. (US) Spec. Publ., 341, 67 (1970).

SECTION 10

TECHNICAL REPORT SUMMARY

This is the first semiannual report for a program that is directed toward the development of a nondestructive method to predict laser surface damage of transparent dielectric materials used in high power laser systems. Very high peak power laser systems are being developed for application in ordnance, communication, and thermonuclear fusion. The test program includes (1) investigation of exoelectron properties of a series of selected laser optical materials after exposure to ionizing radiation or to high peak power laser pulses, (2) correlation of exoelectron images, obtained after exposure of the surface to laser pulses, with laser surface damage characteristics of these surfaces, and (3) study of the feasibility of using exoelectron surface imaging as a technique to nondestructively predict the laser surface damage threshold of laser optical materials.

All test facilities required for this program were developed. Our work on EE emission from laser glass indicated that exoelectron emission from this type of material is too weak and irreproducible to be of any value. Experiments performed on pyroelectric $LiNbO_3$ resulted in the discovery of thermally-stimulated field emission (TSFE). A theoretical analysis of TSFE revealed that a very high electric field could exist on the surface of $LiNbO_3$ due to a small temperature change in the material. A small temperature increase is easily produced by high peak power laser pulses. The fields produced in this way are capable of contributing significantly to laser surface damage. Therefore, it is important to further investigate this phenomenonon with the goal of understanding the damage mechanism more completely.